Measurement of *CP* violation observables and parameters for the decays $B^{\pm} \to DK^{*\pm}$

B. Aubert,[1] Y. Karyotakis,[1] J. P. Lees,[1] V. Poireau,[1] E. Prencipe,[1] X. Prudent,[1] V. Tisserand,[1] J. Garra Tico,[2] E. Grauges,[2] M. Martinelli,[3a,3b] A. Palano,[3a,3b] M. Pappagallo,[3a,3b] G. Eigen,[4] B. Stugu,[4] L. Sun,[4] M. Battaglia,[5] D. N. Brown,[5] L. T. Kerth,[5] Yu. G. Kolomensky,[5] G. Lynch,[5] I. L. Osipenkov,[5] K. Tackmann,[5] T. Tanabe,[5] C. M. Hawkes,[6] N. Soni,[6] A. T. Watson,[6] H. Koch,[7] T. Schroeder,[7] D. J. Asgeirsson,[8] B. G. Fulsom,[8] C. Hearty,[8] T. S. Mattison,[8] J. A. McKenna,[8] M. Barrett,[9] A. Khan,[9] A. Randle-Conde,[9] V. E. Blinov,[10] A. D. Bukin,[10,*] A. R. Buzykaev,[10] V. P. Druzhinin,[10] V. B. Golubev,[10] A. P. Onuchin,[10] S. I. Serednyakov,[10] Yu. I. Skovpen,[10] E. P. Solodov,[10] K. Yu. Todyshev,[10] M. Bondioli,[11] S. Curry,[11] I. Eschrich,[11] D. Kirkby,[11] A. J. Lankford,[11] P. Lund,[11] M. Mandelkern,[11] E. C. Martin,[11] D. P. Stoker,[11] H. Atmacan,[12] J. W. Gary,[12] F. Liu,[12] O. Long,[12] G. M. Vitug,[12] Z. Yasin,[12] V. Sharma,[13] C. Campagnari,[14] T. M. Hong,[14] D. Kovalskyi,[14] M. A. Mazur,[14] J. D. Richman,[14] T. W. Beck,[15] A. M. Eisner,[15] C. A. Heusch,[15] J. Kroseberg,[15] W. S. Lockman,[15] A. J. Martinez,[15] T. Schalk,[15] B. A. Schumm,[15] A. Seiden,[15] L. Wang,[15] L. O. Winstrom,[15] C. H. Cheng,[16] D. A. Doll,[16] B. Echenard,[16] F. Fang,[16] D. G. Hitlin,[16] I. Narsky,[16] P. Ongmongkolkul,[16] T. Piatenko,[16] F. C. Porter,[16] R. Andreassen,[17] G. Mancinelli,[17] B. T. Meadows,[17] K. Mishra,[17] M. D. Sokoloff,[17] P. C. Bloom,[18] W. T. Ford,[18] A. Gaz,[18] J. F. Hirschauer,[18] M. Nagel,[18] U. Nauenberg,[18] J. G. Smith,[18] S. R. Wagner,[18] R. Ayad,[19,†] W. H. Toki,[19] R. J. Wilson,[19] E. Feltresi,[20] A. Hauke,[20] H. Jasper,[20] T. M. Karbach,[20] J. Merkel,[20] A. Petzold,[20] B. Spaan,[20] K. Wacker,[20] M. J. Kobel,[21] R. Nogowski,[21] K. R. Schubert,[21] R. Schwierz,[21] D. Bernard,[22] E. Latour,[22] M. Verderi,[22] P. J. Clark,[23] S. Playfer,[23] J. E. Watson,[23] M. Andreotti,[24a,24b] D. Bettoni,[24a] C. Bozzi,[24a] R. Calabrese,[24a,24b] A. Cecchi,[24a,24b] G. Cibinetto,[24a,24b] E. Fioravanti,[24a,24b] P. Franchini,[24a,24b] E. Luppi,[24a,24b] M. Munerato,[24a,24b] M. Negrini,[24a,24b] A. Petrella,[24a,24b] L. Piemontese,[24a] V. Santoro,[24a,24b] R. Baldini-Ferroli,[25] A. Calcaterra,[25] R. de Sangro,[25] G. Finocchiaro,[25] S. Pacetti,[25] P. Patteri,[25] I. M. Peruzzi,[25,‡] M. Piccolo,[25] M. Rama,[25] A. Zallo,[25] R. Contri,[26a,26b] E. Guido,[26a,26b] M. Lo Vetere,[26a,26b] M. R. Monge,[26a,26b] S. Passaggio,[26a] C. Patrignani,[26a,26b] E. Robutti,[26a] S. Tosi,[26a,26b] K. S. Chaisanguanthum,[27] M. Morii,[27] A. Adametz,[28] J. Marks,[28] S. Schenk,[28] U. Uwer,[28] F. U. Bernlochner,[29] V. Klose,[29] H. M. Lacker,[29] T. Lueck,[29] A. Volk,[29] D. J. Bard,[30] P. D. Dauncey,[30] M. Tibbetts,[30] P. K. Behera,[31] M. J. Charles,[31] U. Mallik,[31] J. Cochran,[32] H. B. Crawley,[32] L. Dong,[32] V. Eyges,[32] W. T. Meyer,[32] S. Prell,[32] E. I. Rosenberg,[32] A. E. Rubin,[32] Y. Y. Gao,[33] A. V. Gritsan,[33] Z. J. Guo,[33] N. Arnaud,[34] J. Béquilleux,[34] A. D'Orazio,[34] M. Davier,[34] D. Derkach,[34] J. Firmino da Costa,[34] G. Grosdidier,[34] F. Le Diberder,[34] V. Lepeltier,[34] A. M. Lutz,[34] B. Malaescu,[34] S. Pruvot,[34] P. Roudeau,[34] M. H. Schune,[34] J. Serrano,[34] V. Sordini,[34,§] A. Stocchi,[34] G. Wormser,[34] D. J. Lange,[35] D. M. Wright,[35] I. Bingham,[36] J. P. Burke,[36] C. A. Chavez,[36] J. R. Fry,[36] E. Gabathuler,[36] R. Gamet,[36] D. E. Hutchcroft,[36] D. J. Payne,[36] C. Touramanis,[36] A. J. Bevan,[37] C. K. Clarke,[37] F. Di Lodovico,[37] R. Sacco,[37] M. Sigamani,[37] G. Cowan,[38] S. Paramesvaran,[38] A. C. Wren,[38] D. N. Brown,[39] C. L. Davis,[39] A. G. Denig,[40] M. Fritsch,[40] W. Gradl,[40] A. Hafner,[40] K. E. Alwyn,[41] D. Bailey,[41] R. J. Barlow,[41] G. Jackson,[41] G. D. Lafferty,[41] T. J. West,[41] J. I. Yi,[41] J. Anderson,[42] C. Chen,[42] A. Jawahery,[42] D. A. Roberts,[42] G. Simi,[42] J. M. Tuggle,[42] C. Dallapiccola,[43] E. Salvati,[43] R. Cowan,[44] D. Dujmic,[44] P. H. Fisher,[44] S. W. Henderson,[44] G. Sciolla,[44] M. Spitznagel,[44] R. K. Yamamoto,[44] M. Zhao,[44] P. M. Patel,[45] S. H. Robertson,[45] M. Schram,[45] P. Biassoni,[46a,46b] A. Lazzaro,[46a,46b] V. Lombardo,[46a] F. Palombo,[46a,46b] S. Stracka,[46a,46b] L. Cremaldi,[47] R. Godang,[47,‖] R. Kroeger,[47] P. Sonnek,[47] D. J. Summers,[47] H. W. Zhao,[47] M. Simard,[48] P. Taras,[48] H. Nicholson,[49] G. De Nardo,[50a,50b] L. Lista,[50a] D. Monorchio,[50a,50b] G. Onorato,[50a,50b] C. Sciacca,[50a,50b] G. Raven,[51] H. L. Snoek,[51] C. P. Jessop,[52] K. J. Knoepfel,[52] J. M. LoSecco,[52] W. F. Wang,[52] G. Benelli,[53] L. A. Corwin,[53] K. Honscheid,[53] H. Kagan,[53] R. Kass,[53] J. P. Morris,[53] A. M. Rahimi,[53] S. J. Sekula,[53] Q. K. Wong,[53] N. L. Blount,[54] J. Brau,[54] R. Frey,[54] O. Igonkina,[54] J. A. Kolb,[54] M. Lu,[54] R. Rahmat,[54] N. B. Sinev,[54] D. Strom,[54] J. Strube,[54] E. Torrence,[54] G. Castelli,[55a,55b] N. Gagliardi,[55a,55b] M. Margoni,[55a,55b] M. Morandin,[55a] M. Posocco,[55a] M. Rotondo,[55a] F. Simonetto,[55a,55b] R. Stroili,[55a,55b] C. Voci,[55a,55b] P. del Amo Sanchez,[56] E. Ben-Haim,[56] G. R. Bonneaud,[56] H. Briand,[56] J. Chauveau,[56] O. Hamon,[56] Ph. Leruste,[56] G. Marchiori,[56] J. Ocariz,[56] A. Perez,[56] J. Prendki,[56] S. Sitt,[56] L. Gladney,[57] M. Biasini,[58a,58b] E. Manoni,[58a,58b] C. Angelini,[59a,59b] G. Batignani,[59a,59b] S. Bettarini,[59a,59b] G. Calderini,[59a,59b,¶] M. Carpinelli,[59a,59b,**] A. Cervelli,[59a,59b] F. Forti,[59a,59b] M. A. Giorgi,[59a,59b] A. Lusiani,[59a,59c] M. Morganti,[59a,59b] N. Neri,[59a,59b] E. Paoloni,[59a,59b] G. Rizzo,[59a,59b] J. J. Walsh,[59a] D. Lopes Pegna,[60] C. Lu,[60] J. Olsen,[60] A. J. S. Smith,[60] A. V. Telnov,[60] F. Anulli,[61a] E. Baracchini,[61a,61b] G. Cavoto,[61a] R. Faccini,[61a,61b] F. Ferrarotto,[61a] F. Ferroni,[61a,61b] M. Gaspero,[61a,61b] P. D. Jackson,[61a] L. Li Gioi,[61a] M. A. Mazzoni,[61a] S. Morganti,[61a] G. Piredda,[61a] F. Renga,[61a,61b] C. Voena,[61a] M. Ebert,[62] T. Hartmann,[62] H. Schröder,[62] R. Waldi,[62] T. Adye,[63] B. Franek,[63] E. O. Olaiya,[63] F. F. Wilson,[63] S. Emery,[64] L. Esteve,[64] G. Hamel de Monchenault,[64] W. Kozanecki,[64] G. Vasseur,[64] Ch. Yèche,[64] M. Zito,[64] M. T. Allen,[65] D. Aston,[65] R. Bartoldus,[65] J. F. Benitez,[65]

R. Cenci,[65] J. P. Coleman,[65] M. R. Convery,[65] J. C. Dingfelder,[65] J. Dorfan,[65] G. P. Dubois-Felsmann,[65] W. Dunwoodie,[65] R. C. Field,[65] M. Franco Sevilla,[65] A. M. Gabareen,[65] M. T. Graham,[65] P. Grenier,[65] C. Hast,[65] W. R. Innes,[65] J. Kaminski,[65] M. H. Kelsey,[65] H. Kim,[65] P. Kim,[65] M. L. Kocian,[65] D. W. G. S. Leith,[65] S. Li,[65] B. Lindquist,[65] S. Luitz,[65] V. Luth,[65] H. L. Lynch,[65] D. B. MacFarlane,[65] H. Marsiske,[65] R. Messner,[65,*] D. R. Muller,[65] H. Neal,[65] S. Nelson,[65] C. P. O'Grady,[65] I. Ofte,[65] M. Perl,[65] B. N. Ratcliff,[65] A. Roodman,[65] A. A. Salnikov,[65] R. H. Schindler,[65] J. Schwiening,[65] A. Snyder,[65] D. Su,[65] M. K. Sullivan,[65] K. Suzuki,[65] S. K. Swain,[65] J. M. Thompson,[65] J. Va'vra,[65] A. P. Wagner,[65] M. Weaver,[65] C. A. West,[65] W. J. Wisniewski,[65] M. Wittgen,[65] D. H. Wright,[65] H. W. Wulsin,[65] A. K. Yarritu,[65] C. C. Young,[65] V. Ziegler,[65] X. R. Chen,[66] H. Liu,[66] W. Park,[66] M. V. Purohit,[66] R. M. White,[66] J. R. Wilson,[66] M. Bellis,[67] P. R. Burchat,[67] A. J. Edwards,[67] T. S. Miyashita,[67] S. Ahmed,[68] M. S. Alam,[68] J. A. Ernst,[68] B. Pan,[68] M. A. Saeed,[68] S. B. Zain,[68] A. Soffer,[69] S. M. Spanier,[70] B. J. Wogsland,[70] R. Eckmann,[71] J. L. Ritchie,[71] A. M. Ruland,[71] C. J. Schilling,[71] R. F. Schwitters,[71] B. C. Wray,[71] B. W. Drummond,[72] J. M. Izen,[72] X. C. Lou,[72] F. Bianchi,[73a,73b] D. Gamba,[73a,73b] M. Pelliccioni,[73a,73b] M. Bomben,[74a,74b] L. Bosisio,[74a,74b] C. Cartaro,[74a,74b] G. Della Ricca,[74a,74b] L. Lanceri,[74a,74b] L. Vitale,[74a,74b] V. Azzolini,[75] N. Lopez-March,[75] F. Martinez-Vidal,[75] D. A. Milanes,[75] A. Oyanguren,[75] J. Albert,[76] Sw. Banerjee,[76] B. Bhuyan,[76] H. H. F. Choi,[76] K. Hamano,[76] G. J. King,[76] R. Kowalewski,[76] M. J. Lewczuk,[76] I. M. Nugent,[76] J. M. Roney,[76] R. J. Sobie,[76] T. J. Gershon,[77] P. F. Harrison,[77] J. Ilic,[77] T. E. Latham,[77] G. B. Mohanty,[77] E. M. T. Puccio,[77] H. R. Band,[78] X. Chen,[78] S. Dasu,[78] K. T. Flood,[78] Y. Pan,[78] R. Prepost,[78] C. O. Vuosalo,[78] and S. L. Wu[78]

[1]*Laboratoire d'Annecy-le-Vieux de Physique des Particules (LAPP), Université de Savoie, CNRS/IN2P3, F-74941 Annecy-Le-Vieux, France*
[2]*Universitat de Barcelona, Facultat de Fisica, Departament ECM, E-08028 Barcelona, Spain*
[3a]*INFN Sezione di Bari, I-70126 Bari, Italy*
[3b]*Dipartimento di Fisica, Università di Bari, I-70126 Bari, Italy*
[4]*University of Bergen, Institute of Physics, N-5007 Bergen, Norway*
[5]*Lawrence Berkeley National Laboratory and University of California, Berkeley, California 94720, USA*
[6]*University of Birmingham, Birmingham, B15 2TT, United Kingdom*
[7]*Ruhr Universität Bochum, Institut für Experimentalphysik 1, D-44780 Bochum, Germany*
[8]*University of British Columbia, Vancouver, British Columbia, Canada V6T 1Z1*
[9]*Brunel University, Uxbridge, Middlesex UB8 3PH, United Kingdom*
[10]*Budker Institute of Nuclear Physics, Novosibirsk 630090, Russia*
[11]*University of California at Irvine, Irvine, California 92697, USA*
[12]*University of California at Riverside, Riverside, California 92521, USA*
[13]*University of California at San Diego, La Jolla, California 92093, USA*
[14]*University of California at Santa Barbara, Santa Barbara, California 93106, USA*
[15]*University of California at Santa Cruz, Institute for Particle Physics, Santa Cruz, California 95064, USA*
[16]*California Institute of Technology, Pasadena, California 91125, USA*
[17]*University of Cincinnati, Cincinnati, Ohio 45221, USA*
[18]*University of Colorado, Boulder, Colorado 80309, USA*
[19]*Colorado State University, Fort Collins, Colorado 80523, USA*
[20]*Technische Universität Dortmund, Fakultät Physik, D-44221 Dortmund, Germany*
[21]*Technische Universität Dresden, Institut für Kern- und Teilchenphysik, D-01062 Dresden, Germany*
[22]*Laboratoire Leprince-Ringuet, CNRS/IN2P3, Ecole Polytechnique, F-91128 Palaiseau, France*
[23]*University of Edinburgh, Edinburgh EH9 3JZ, United Kingdom*
[24a]*INFN Sezione di Ferrara, I-44100 Ferrara, Italy*
[24b]*Dipartimento di Fisica, Università di Ferrara, I-44100 Ferrara, Italy*
[25]*INFN Laboratori Nazionali di Frascati, I-00044 Frascati, Italy*
[26a]*INFN Sezione di Genova, I-16146 Genova, Italy*
[26b]*Dipartimento di Fisica, Università di Genova, I-16146 Genova, Italy*
[27]*Harvard University, Cambridge, Massachusetts 02138, USA*
[28]*Universität Heidelberg, Physikalisches Institut, Philosophenweg 12, D-69120 Heidelberg, Germany*
[29]*Humboldt-Universität zu Berlin, Institut für Physik, Newtonstr. 15, D-12489 Berlin, Germany*
[30]*Imperial College London, London, SW7 2AZ, United Kingdom*
[31]*University of Iowa, Iowa City, Iowa 52242, USA*
[32]*Iowa State University, Ames, Iowa 50011-3160, USA*
[33]*Johns Hopkins University, Baltimore, Maryland 21218, USA*
[34]*Laboratoire de l'Accélérateur Linéaire, IN2P3/CNRS et Université Paris-Sud 11, Centre Scientifique d'Orsay, B. P. 34, F-91898 Orsay Cedex, France*
[35]*Lawrence Livermore National Laboratory, Livermore, California 94550, USA*

[36]*University of Liverpool, Liverpool L69 7ZE, United Kingdom*
[37]*Queen Mary, University of London, London, E1 4NS, United Kingdom*
[38]*University of London, Royal Holloway and Bedford New College, Egham, Surrey TW20 0EX, United Kingdom*
[39]*University of Louisville, Louisville, Kentucky 40292, USA*
[40]*Johannes Gutenberg-Universität Mainz, Institut für Kernphysik, D-55099 Mainz, Germany*
[41]*University of Manchester, Manchester M13 9PL, United Kingdom*
[42]*University of Maryland, College Park, Maryland 20742, USA*
[43]*University of Massachusetts, Amherst, Massachusetts 01003, USA*
[44]*Massachusetts Institute of Technology, Laboratory for Nuclear Science, Cambridge, Massachusetts 02139, USA*
[45]*McGill University, Montréal, Québec, Canada H3A 2T8*
[46a]*INFN Sezione di Milano, I-20133 Milano, Italy*
[46b]*Dipartimento di Fisica, Università di Milano, I-20133 Milano, Italy*
[47]*University of Mississippi, University, Mississippi 38677, USA*
[48]*Université de Montréal, Physique des Particules, Montréal, Québec, Canada H3C 3J7*
[49]*Mount Holyoke College, South Hadley, Massachusetts 01075, USA*
[50a]*INFN Sezione di Napoli, I-80126 Napoli, Italy*
[50b]*Dipartimento di Scienze Fisiche, Università di Napoli Federico II, I-80126 Napoli, Italy*
[51]*NIKHEF, National Institute for Nuclear Physics and High Energy Physics, NL-1009 DB Amsterdam, The Netherlands*
[52]*University of Notre Dame, Notre Dame, Indiana 46556, USA*
[53]*Ohio State University, Columbus, Ohio 43210, USA*
[54]*University of Oregon, Eugene, Oregon 97403, USA*
[55a]*INFN Sezione di Padova, I-35131 Padova, Italy*
[55b]*Dipartimento di Fisica, Università di Padova, I-35131 Padova, Italy*
[56]*Laboratoire de Physique Nucléaire et de Hautes Energies, IN2P3/CNRS, Université Pierre et Marie Curie-Paris6, Université Denis Diderot-Paris7, F-75252 Paris, France*
[57]*University of Pennsylvania, Philadelphia, Pennsylvania 19104, USA*
[58a]*INFN Sezione di Perugia, I-06100 Perugia, Italy*
[58b]*Dipartimento di Fisica, Università di Perugia, I-06100 Perugia, Italy*
[59a]*INFN Sezione di Pisa, I-56127 Pisa, Italy*
[59b]*Dipartimento di Fisica, Università di Pisa, I-56127 Pisa, Italy*
[59c]*Scuola Normale Superiore di Pisa, I-56127 Pisa, Italy*
[60]*Princeton University, Princeton, New Jersey 08544, USA*
[61a]*INFN Sezione di Roma, I-00185 Roma, Italy*
[61b]*Dipartimento di Fisica, Università di Roma La Sapienza, I-00185 Roma, Italy*
[62]*Universität Rostock, D-18051 Rostock, Germany*
[63]*Rutherford Appleton Laboratory, Chilton, Didcot, Oxon, OX11 0QX, United Kingdom*
[64]*CEA, Irfu, SPP, Centre de Saclay, F-91191 Gif-sur-Yvette, France*
[65]*SLAC National Accelerator Laboratory, Stanford, California 94309 USA*
[66]*University of South Carolina, Columbia, South Carolina 29208, USA*
[67]*Stanford University, Stanford, California 94305-4060, USA*
[68]*State University of New York, Albany, New York 12222, USA*
[69]*Tel Aviv University, School of Physics and Astronomy, Tel Aviv, 69978, Israel*
[70]*University of Tennessee, Knoxville, Tennessee 37996, USA*
[71]*University of Texas at Austin, Austin, Texas 78712, USA*
[72]*University of Texas at Dallas, Richardson, Texas 75083, USA*
[73a]*INFN Sezione di Torino, I-10125 Torino, Italy*
[73b]*Dipartimento di Fisica Sperimentale, Università di Torino, I-10125 Torino, Italy*
[74a]*INFN Sezione di Trieste, I-34127 Trieste, Italy*
[74b]*Dipartimento di Fisica, Università di Trieste, I-34127 Trieste, Italy*
[75]*IFIC, Universitat de Valencia-CSIC, E-46071 Valencia, Spain*
[76]*University of Victoria, Victoria, British Columbia, Canada V8W 3P6*

[*]Deceased.
[†]Present address: Temple University, Philadelphia, PA 19122, USA.
[‡]Also with Università di Perugia, Dipartimento di Fisica, Perugia, Italy.
[§]Also with Università di Roma La Sapienza, I-00185 Roma, Italy.
[‖]Present address: University of South Alabama, Mobile, AL 36688, USA.
[¶]Also with Laboratoire de Physique Nucléaire et de Hautes Energies, IN2P3/CNRS, Université Pierre et Marie Curie-Paris6, Université Denis Diderot-Paris7, F-75252 Paris, France.
[**]Also with Università di Sassari, Sassari, Italy.

[77]*Department of Physics, University of Warwick, Coventry CV4 7AL, United Kingdom*
[78]*University of Wisconsin, Madison, Wisconsin 53706, USA*
(Received 23 September 2009; published 3 November 2009)

We study the decay $B^- \to DK^{*-}$ using a sample of 379×10^6 $\Upsilon(4S) \to B\bar{B}$ events collected with the *BABAR* detector at the PEP-II B factory. We perform a Gronau-London-Wyler analysis where the D meson decays into either a CP-even ($CP+$) eigenstate (K^+K^-, $\pi^+\pi^-$), CP-odd ($CP-$) eigenstate ($K^0_S\pi^0$, $K^0_S\phi$, $K^0_S\omega$) or a non-CP state ($K^-\pi^+$). We also analyze D meson decays into $K^+\pi^-$ from a Cabibbo-favored $\bar{D}^0$ decay or doubly suppressed D^0 decay [Atwood-Dunietz-Soni (ADS) analysis]. We measure observables that are sensitive to the Cabibbo-Kobayashi-Maskawa angle γ: the partial-rate charge asymmetries $\mathcal{A}_{CP\pm}$, the ratios $\mathcal{R}_{CP\pm}$ of the B-decay branching fractions in $CP\pm$ and non-CP decay, the ratio $\mathcal{R}_{\rm ADS}$ of the charge-averaged branching fractions, and the charge asymmetry $\mathcal{A}_{\rm ADS}$ of the ADS decays: $\mathcal{A}_{CP+} = 0.09 \pm 0.13 \pm 0.06$, $\mathcal{A}_{CP-} = -0.23 \pm 0.21 \pm 0.07$, $\mathcal{R}_{CP+} = 2.17 \pm 0.35 \pm 0.09$, $\mathcal{R}_{CP-} = 1.03 \pm 0.27 \pm 0.13$, $\mathcal{R}_{\rm ADS} = 0.066 \pm 0.031 \pm 0.010$, and $\mathcal{A}_{\rm ADS} = -0.34 \pm 0.43 \pm 0.16$, where the first uncertainty is statistical and the second is systematic. Combining all the measurements and using a frequentist approach yields the magnitude of the ratio between the Cabibbo-suppressed and favored amplitudes, $r_B = 0.31$ with a one (two) sigma confidence level interval of [0.24, 0.38] ([0.17, 0.43]). The value $r_B = 0$ is excluded at the 3.3 sigma level. A similar analysis excludes values of γ in the intervals [0, 7]°, [55, 111]°, and [175, 180]° ([85, 99]°) at the one (two) sigma confidence level.

DOI: 10.1103/PhysRevD.80.092001 PACS numbers: 13.25.Hw, 11.30.Er, 12.15.Hh, 14.40.Nd

I. INTRODUCTION

The standard model accommodates CP violation through a single phase in the Cabibbo-Kobayashi-Maskawa (CKM) quark mixing matrix V [1]. The self-consistency of this mechanism can be tested by overconstraining the associated unitarity triangle [2,3] using many different measurements, mostly involving decays of B mesons. In this paper we concentrate on the angle $\gamma \equiv \arg(-V_{ud}V^*_{ub}/V_{cd}V^*_{cb})$ by studying B meson decay channels where $b \to c\bar{u}s$ and $b \to u\bar{c}s$ tree amplitudes interfere. We use two techniques, one suggested by Gronau and London [4] and Gronau and Wyler [5] (GLW) and the other suggested by Atwood, Dunietz, and Soni [6] (ADS) to study γ. Both techniques rely on final states that can be reached from both D^0 and $\bar{D}^0$ decays. These methods make use of B decay amplitudes that involve standard model tree diagrams, and therefore yield theoretically clean measurements of γ. As discussed in Ref. [7] the combination of the GLW and ADS observables can be very useful in resolving certain ambiguities inherent in each of the techniques. In this paper we use the decay $B^- \to DK^{*-}(892)$ [8] to measure the GLW and ADS observables.

In the GLW analysis the D meson [9] from $B^- \to DK^{*-}$ decays into either a CP-even ($CP+$) eigenstate (K^+K^-, $\pi^+\pi^-$) or a CP-odd ($CP-$) eigenstate ($K_s\pi^0$, $K_s\phi$, $K_s\omega$). The size of the interference between the two competing amplitudes depends on the CKM angle γ as well as other parameters that are CP conserving, discussed below. References [4,5] define several observables that depend on measurable quantities:

$$\mathcal{R}_{CP\pm} = 2\frac{\Gamma(B^- \to D^0_{CP^\pm}K^{*-}) + \Gamma(B^+ \to D^0_{CP^\pm}K^{*+})}{\Gamma(B^- \to D^0_{K\pi}K^{*-}) + \Gamma(B^+ \to \bar{D}^0_{K\pi}K^{*+})},$$

$$\mathcal{A}_{CP\pm} = \frac{\Gamma(B^- \to D^0_{CP^\pm}K^{*-}) - \Gamma(B^+ \to D^0_{CP^\pm}K^{*+})}{\Gamma(B^- \to D^0_{CP^\pm}K^{*-}) + \Gamma(B^+ \to D^0_{CP^\pm}K^{*+})}.$$

Here $D^0_{CP\pm}$ refers to a neutral D meson decaying into either a $CP+$ or $CP-$ eigenstate.

$\mathcal{R}_{CP\pm}$ and $\mathcal{A}_{CP\pm}$ depend on the physical parameters as follows:

$$\mathcal{R}_{CP\pm} = 1 + r_B^2 \pm 2r_B\cos\delta_B\cos\gamma, \quad (1)$$

$$\mathcal{A}_{CP\pm} = \pm 2r_B\sin\delta_B\sin\gamma/\mathcal{R}_{CP\pm}. \quad (2)$$

Here r_B is the magnitude of the ratio of the suppressed $B^- \to \bar{D}^0K^{*-}$ and favored $B^- \to D^0K^{*-}$ decay amplitudes, respectively, and δ_B is the CP-conserving phase difference between these amplitudes. In this analysis we neglect the effects of CP violation in D meson decays, and, as justified in Ref. [10], the very small effect of $D^0\bar{D}^0$ mixing.

$\mathcal{R}_{CP\pm}$ is calculated using

$$\mathcal{R}_{CP\pm} = \frac{N_{CP\pm}}{N_{\text{non}-CP}} \times \frac{\epsilon_{\text{non}-CP}}{\epsilon_{CP\pm}} \quad (3)$$

where $N_{CP\pm}$ and $N_{\text{non-}CP}$ are the event yields for the CP and non-CP modes, respectively, and $\epsilon_{\text{non-}CP}$ and $\epsilon_{CP\pm}$ are correction factors that depend on branching fractions and reconstruction efficiencies. $\mathcal{A}_{CP\pm}$ is calculated using the event yields split by the charge of the B meson.

We define two additional quantities whose experimental estimators are normally distributed even when the value of r_B is comparable to its uncertainty:

$$x_\pm = r_B \cos(\delta_B \pm \gamma) = \frac{R_{CP+}(1 \mp \mathcal{A}_{CP+}) - R_{CP-}(1 \mp \mathcal{A}_{CP-})}{4}. \quad (4)$$

Since $x_\pm$ are also directly measured in Dalitz-plot analyses [11], the different results can be compared and combined with each other. We note that an additional set of quantities measured in Dalitz-plot analyses, $y_\pm = r_B \sin(\delta_B \pm \gamma)$, are not directly accessible through the GLW analysis.

In the ADS technique, $B^- \to DK^{*-}$ decays to $[K^+\pi^-]_D K^{*-}$, where $[K^+\pi^-]_D$ indicates that these particles are neutral D meson (D^0 or $\bar{D}^0$) decay products. This final state can be reached from $B \to D^0 K^{*-}$ and the doubly-Cabibbo-suppressed decay $D^0 \to K^+\pi^-$ or $B^- \to \bar{D}^0 K^{*-}$ followed by the Cabibbo-favored decay $\bar{D}^0 \to K^+\pi^-$. In addition, the final state $[K^-\pi^+]_D K^{*-}$ is used for normalization. We label the decays where the K and K^* have the same (opposite) charge as "right (wrong) sign" where the labels reflect that one mode occurs much more often than the other.

In analogy with the GLW method we define two measurable quantities, $\mathcal{R}_{\rm ADS}$ and $\mathcal{A}_{\rm ADS}$, as follows:

$$\mathcal{R}_{\rm ADS} = \frac{\Gamma(B^- \to [K^+\pi^-]_D K^{*-}) + \Gamma(B^+ \to [K^-\pi^+]_D K^{*+})}{\Gamma(B^- \to [K^-\pi^+]_D K^{*-}) + \Gamma(B^+ \to [K^+\pi^-]_D K^{*+})},$$
$$\mathcal{A}_{\rm ADS} = \frac{\Gamma(B^- \to [K^+\pi^-]_D K^{*-}) - \Gamma(B^+ \to [K^-\pi^+]_D K^{*+})}{\Gamma(B^- \to [K^+\pi^-]_D K^{*-}) + \Gamma(B^+ \to [K^-\pi^+]_D K^{*+})}.$$

$\mathcal{R}_{\rm ADS}$ and $\mathcal{A}_{\rm ADS}$ are related to physically interesting quantities by

$$\mathcal{R}_{\rm ADS} = r_D^2 + r_B^2 + 2 r_D r_B \cos(\delta_B + \delta_D)\cos\gamma, \quad (5)$$

$$\mathcal{A}_{\rm ADS} = 2 r_D r_B \sin(\delta_B + \delta_D)\sin\gamma / \mathcal{R}_{\rm ADS}. \quad (6)$$

Here r_D is the magnitude of the ratio of suppressed $D^0 \to K^+\pi^-$ and favored $D^0 \to K^-\pi^+$ decay amplitudes, respectively, while δ_D is the CP-conserving strong phase difference between these two amplitudes. Both r_D and δ_D have been measured and we use the values given in Ref. [12]: $r_D = 0.0578 \pm 0.0008$ and $\delta_D = 21.9^{+11.3}_{-12.4}$ degrees. Estimates for r_B are in the range $0.1 \le r_B \le 0.3$ [13,14].

It has been pointed out in Ref. [13] that complications due to possible variations in r_B and/or δ_B as a result of the finite width of a resonance such as the K^* and its overlap with other states can be taken into account using an alternate formalism. However, in this paper we choose to follow the procedures in Refs. [14,15] and incorporate the effects of the non-K^* $DK\pi$ events and finite width of the K^* into the systematic uncertainties of our $\mathcal{A}$ and $\mathcal{R}$ measurements.

II. THE *BABAR* DETECTOR AND DATA SET

The *BABAR* detector has been described in detail in Ref. [16] and therefore will only be briefly discussed here. The trajectories of charged tracks are measured with a five-layer double-sided silicon vertex tracker (SVT) and a 40-layer drift chamber (DCH). Both the SVT and DCH are located inside a 1.5 T magnetic field. Photons are detected by means of a CsI(Tl) crystal calorimeter also located inside the magnet. Charged particle identification is determined from information provided by a ring-imaging Cherenkov device (DIRC) in combination with ionization measurements (dE/dx) from the tracking detectors. The *BABAR* detector's response to various physics processes as well as varying beam and environmental conditions is modeled with simulation software based on the GEANT4 [17] tool kit. We use EVTGEN [18] to model the kinematics of B mesons and JETSET [19] to model continuum processes ($e^+e^- \to c\bar{c}, u\bar{u}, d\bar{d}, s\bar{s}$). This analysis uses data collected at and near the $\Upsilon(4S)$ resonance with the *BABAR* detector at the PEP-II storage ring. The data set consists of 345 fb^{-1} collected at the peak of the $\Upsilon(4S)$ (379×10^6 $B\bar{B}$ pairs) and 35 fb^{-1} collected 40 MeV below the resonance peak (off-peak data).

This analysis is a combined update of the previous *BABAR* ADS [14] and GLW [15] studies of $B^- \to DK^{*-}$, which used 232×10^6 $B\bar{B}$ pairs. Other new features in this analysis include the improvement in background suppression, the refinement of various candidate selection criteria, and an update of the estimation of systematic uncertainties. The major change is the choice of neural networks in the GLW analysis over Fisher discriminants, which were used in the previous analysis. We verify the improvements on both signal efficiency and continuum background rejection in the GLW decay channels with simulated signal and continuum events. The increases in signal efficiency range from 3% to 14% for all channels except $K^0_S\phi$, which has the same efficiency. For continuum suppression, the neural networks perform 10% to 57% better across all channels except K^+K^-, which displays the same performance.

III. THE GLW ANALYSIS

We reconstruct $B^- \to DK^{*-}$ candidates with the subsequent decays $K^{*-} \to K^0_S\pi^-$, $K^0_S \to \pi^+\pi^-$ and with the D meson decaying into six decay final states: $D^0 \to K^-\pi^+$ (non-CP final state); K^+K^-, $\pi^+\pi^-$ ($CP+$ eigenstates); and $K^0_S\pi^0$, $K^0_S\phi$, $K^0_S\omega$ ($CP-$ eigenstates). We optimize our event selection criteria by maximizing the figure of merit $S/\sqrt{S+B}$, with S the number of signal events and B the number of background events, determined for each channel using simulated signal and background events. Kaon and pion candidates (except for the pions from K^0_S decays) are selected using a likelihood-based particle-identification algorithm which relies on dE/dx information measured in the DCH and the SVT, and Cherenkov photons in the DIRC. The efficiencies of the selectors are typically above 85% for momenta below 4 GeV while the kaon and pion misidentification rates are at the few percent level for particles in this momentum range.

The K^0_S candidates are formed from oppositely charged tracks assumed to be pions with a reconstructed invariant mass within 13 MeV/c^2 (4 standard deviations) of the known K^0_S mass [3], $m_{K^0_S}$. All K^0_S candidates are refitted so that their invariant mass equals $m_{K^0_S}$ (mass constraint). They are also constrained to emerge from a single vertex (vertex constraint). For those retained to build a K^{*-} candidate, we further require that their flight direction and length be consistent with a K^0_S coming from the interaction point. The K^0_S candidate flight path and momentum vectors must make an acute angle and the flight length in the plane transverse to the beam direction must exceed its uncertainty by 3 standard deviations. K^{*-} candidates are formed from a K^0_S and a charged particle with a vertex constraint. We select K^{*-} candidates that have an invariant mass within 75 MeV/c^2 of the known mean value for a K^* [3]. Finally, since the K^{*-} in $B^- \to DK^{*-}$ is longitudinally polarized, we require $|\cos\theta_H| \geq 0.35$, where θ_H is the angle in the K^{*-} rest frame between the daughter pion momentum and the parent B momentum. The helicity distribution discriminates well between a B-meson decay and a false B-meson candidate from the continuum, since the former is distributed as $\cos^2\theta_H$ and the latter has an approximately flat distribution.

Some decay modes of the D meson contain a neutral pion. We combine pairs of photons to form π^0 candidates with a total energy greater than 200 MeV and an invariant mass between 115 and 150 MeV/c^2. A mass constrained fit is applied to the selected π^0 candidate momenta. Composite particles (ϕ and ω) included in the $CP-$ modes are vertex constrained. Candidate ϕ (ω) mesons are constructed from K^+K^- ($\pi^+\pi^-\pi^0$) particle combinations with an invariant mass required to be within 2 standard deviations, corresponding to 12(20) MeV/c^2, from the known peak values [3]. Two further requirements are made on the ω candidates. The magnitude of the cosine of the helicity angle θ_H between the D momentum in the rest frame of the ω and the normal to the plane containing all three decay pions must be greater than 0.35 (this variable has a $\cos^2\theta_H$ distribution for signal candidates and is approximately flat for background). The Dalitz angle [20] θ_D is defined as the angle between the momentum of one daughter pion in the ω rest frame and the direction of one of the other two pions in the rest frame of the two pions. For signal candidates, the cosine of the Dalitz angle follows a $\sin^2\theta_D$ distribution, while it is approximately flat for the background. Therefore we require the cosine of the Dalitz angle of signal candidates to have a magnitude smaller than 0.8.

All D candidates are mass constrained and, with the exception of the $K^0_S\pi^0$ final state, vertex constrained. We select D candidates with an invariant mass differing from the known mass [3] by less than 12 MeV/c^2 for all channels except $K^0_S\pi^0$ (30 MeV/c^2) and $K^0_S\omega$ (20 MeV/c^2). These limits are about twice the corresponding rms mass resolutions.

Suppression of backgrounds from continuum events is achieved by using event-shape and angular variables. The B meson candidate is required to have $|\cos\theta_T| \leq 0.9$, where θ_T is the angle between the thrust axis of the B meson and that of the rest of the event. The distribution of $|\cos\theta_T|$ is uniform in $B\bar{B}$ events and strongly peaked near 1 for continuum events.

A neural network (NN) is used to further reduce the $e^+e^- \to q\bar{q}$ ($q = u, d, s, c$) contribution to our data sample. Seven variables are used in the NN with three being the angular moments L_0, L_1, and L_2. These moments are defined by $L_j = \sum_i p_i^* |\cos\theta_i^*|^j$ where the sum is over charged and neutral particles are not associated with the B-meson candidate. Here p_i^* (θ_i^*) is the momentum (angle) of the ith particle with respect to the thrust of the candidate B meson in the center-of-mass (CM) frame. Additional details on the moments can be found in Ref. [21]. The NN also uses the ratio $R_2 = H_2/H_0$ of Fox-Wolfram moments [22], the cosine of the angle between the B candidate momentum vector and the beam axis ($\cos\theta_B$), $\cos\theta_T$ (defined above), and the cosine of the angle between a D daughter momentum vector in the D rest frame and the direction of the D in the B meson rest frame ($\cos\theta_H(D)$). The distributions of all the above variables show distinct differences between signal and continuum events and thus can be exploited by a NN to preferentially select $B\bar{B}$ events. Each decay mode has its own unique NN trained with signal and continuum Monte Carlo events. After training, the NNs are then fed with independent sets of signal and continuum Monte Carlo events to produce NN outputs for each decay mode. Finally, we verify that the NNs have consistent outputs for off-peak data [continuum data collected below the $\Upsilon(4S)$] and $q\bar{q}$ Monte Carlo events. The separations between signal and continuum backgrounds are shown in Fig. 1. We select candidates

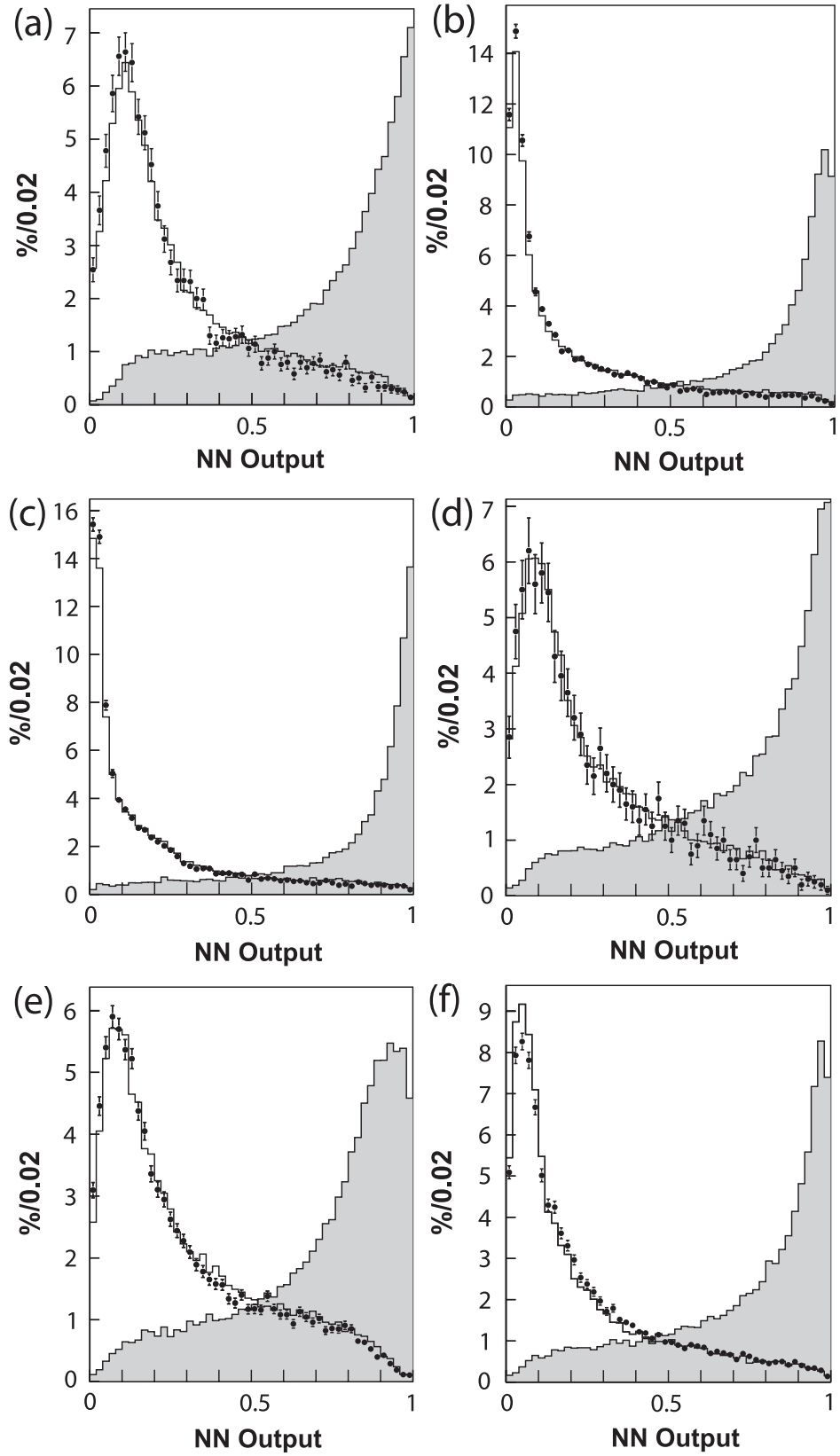

FIG. 1. Neural network (NN) outputs and results of the NN verifications of (a) K^+K^-, (b) $\pi^+\pi^-$, (c) $K^0_S\pi^0$, (d) $K^0_S\phi$, (e) $K^0_S\omega$, and (f) $K^-\pi^+$ subsamples of the GLW analysis. The samples used to produce the output are shown as histograms. The signal (Monte Carlo simulation) is the shaded histogram peaking near 1; the continuum (Monte Carlo simulation) is the histogram peaking near 0. The off-peak data used to check the NN are overlaid as data points.

with neural network output above 0.65 (K^+K^-), 0.82 ($\pi^+\pi^-$), 0.91 ($K^0_S\pi^0$), 0.56 ($K^0_S\phi$), 0.80 ($K^0_S\omega$), and 0.73 ($K^-\pi^+$). Our event selection is optimized to maximize the significance of the signal yield, determined using simulated signal and background events.

We identify B candidates using two nearly independent kinematic variables: the beam-energy-substituted (ES) mass $m_{\rm ES} = \sqrt{(s/2 + \mathbf{p}_0 \cdot \mathbf{p}_B)^2/E_0^2 - p_B^2}$ and the energy difference $\Delta E = E_B^* - \sqrt{s}/2$, where E and p are energy and momentum. The subscripts 0 and B refer to the e^+e^--beam system and the B candidate, respectively; s is the square of the CM energy and the asterisk labels the CM frame. The $m_{\rm ES}$ distributions are all described by a Gaussian function $\mathcal{G}$ centered at the B mass with a resolution (sigma) of 2.50, 2.55, and 2.51 MeV$/c^2$ for the $CP+$, $CP-$, and non-CP mode, respectively. The ΔE distributions are centered on zero for signal with a resolution of 11 to 13 MeV for all channels except $K^0_S\pi^0$ for which the resolution is asymmetric and is about 30 MeV. We define a signal region through the requirement $|\Delta E| < 50(25)$ MeV for $K^0_S\pi^0$ (all other modes).

A potentially dangerous background for the $B^- \to D(\pi^+\pi^-)K^{*-}(K^0_S\pi^-)$ channel is the decay mode $B^- \to D(K^0_S\pi^+\pi^-)\pi^-$ which contains the same final-state particles as the signal but has a branching fraction 600 times larger. We therefore explicitly veto any selected B candidate containing a $K^0_S\pi^+\pi^-$ combination within 60 MeV$/c^2$ of the D^0 mass.

The fraction of events with more than one acceptable B candidate depends on the D decay mode and is always less than 8%. To select the best B candidate in those events where we find more than one acceptable candidate, we choose the one with the smallest χ^2 formed from the differences of the measured and world average D^0 and K^{*-} masses divided by the mass spread that includes the resolution and, for the K^{*-}, the natural width:

$$\chi^2 = \chi^2_{M_{D^0}} + \chi^2_{M_{K^{*-}}} = \frac{(M_{D^0} - M^{\rm PDG}_{D^0})^2}{\sigma^2_{M_{D^0}}} + \frac{(M_{K^{*-}} - M^{\rm PDG}_{K^{*-}})^2}{\sigma^2_{M_{K^{*-}}} + \Gamma^2_{K^{*-}}/c^4}. \quad (7)$$

Simulations show that negligible bias is introduced by this choice and the correct candidate is picked at least 86% of the time.

From the simulation of signal events, the total reconstruction efficiencies are 12.8% and 12.3% for the $CP+$ modes $D \to K^+K^-$ and $\pi^+\pi^-$; 5.6%, 8.9%, and 2.4% for the $CP-$ modes $D \to K^0_S\pi^0$, $K^0_S\phi$, and $K^0_S\omega$; 12.8% for the non-CP mode $D^0 \to K^-\pi^+$.

To study $B\bar{B}$ backgrounds we look in sideband regions in ΔE and m_D. We define the ΔE sideband in the interval $60 \le \Delta E \le 200$ MeV for all modes. This region is used to determine the combinatorial background shapes in the signal and m_D sideband. We choose not to use a lower sideband because of the D^*K^* backgrounds in that region. The sideband region in m_D is slightly mode dependent with a typical requirement that m_D differs from the D^0 mass by more than four and less than 10 standard deviations. This region provides sensitivity to background sources which mimic signal both in ΔE and $m_{\rm ES}$ and originate from either charmed or charmless B meson decays that do not contain a true D meson. As many of the possible contributions to this background are not well known, we measure its size by including the m_D sideband in the fit described below.

An unbinned extended maximum likelihood fit to the $m_{\rm ES}$ distributions of selected B candidates in the range $5.2 \le m_{\rm ES} \le 5.3$ GeV$/c^2$ is used to determine signal and background yields. We use the signal yields to calculate the CP-violating quantities $\mathcal{A}_{CP}$ and $\mathcal{R}_{CP}$. We use the same mean and width of the Gaussian function $\mathcal{G}$ to describe the signal shape for all modes considered. The combinatorial background in the $m_{\rm ES}$ distribution is modeled with the so-called "ARGUS" empirical threshold function $\mathcal{A}$ [23]. It is defined as

$$\mathcal{A}(m_{\rm ES}) \propto m_{\rm ES}\sqrt{1 - x^2}\exp^{-\xi(1-x^2)}, \quad (8)$$

where $x = m_{\rm ES}/E_{\rm max}$ and $E_{\rm max}$ is the maximum mass for pair-produced B mesons given the collider beam energies and is fixed in the fit at 5.291 GeV$/c^2$. The ARGUS shape is governed by one parameter ξ that is left free in the fit. We fit simultaneously $m_{\rm ES}$ distributions of nine samples: the non-CP, $CP+$, and $CP-$ samples for (i.) the signal region, (ii.) the m_D sideband, and (iii.) the ΔE sideband. In addition the signal region is divided into two samples according to the charge of the B candidate. We fit three probability density functions (PDF) weighted by the unknown event yields. For the ΔE sideband, we use $\mathcal{A}$. For the m_D sideband (sb) we use $a_{\rm sb} \cdot \mathcal{A} + b_{\rm sb} \cdot \mathcal{G}$, where $\mathcal{G}$ accounts for fake-D candidates. For the signal region PDF, we use $a \cdot \mathcal{A} + b \cdot \mathcal{G} + c \cdot \mathcal{G}$, where b is scaled from $b_{\rm sb}$ with the assumption that the number of fake D background events present in the signal region is equal to the number measured in the m_D sideband scaled by the ratio of the m_D signal-window to sideband widths, and c is the number of $B^\pm \to DK^{*\pm}$ signal events. The non-CP mode sample, with relatively high statistics, helps constrain the PDF shapes for the low statistics CP mode distributions. The ΔE sideband sample helps determine the $\mathcal{A}$ background shape. In total, the fit determines 19 event yields as well as the mean and width of the signal Gaussian and the ARGUS parameter ξ.

Since the values of ξ obtained for each data sample are consistent with each other, albeit with large statistical uncertainties, we have constrained ξ to have the same value for all data samples in the fit. The simulation shows that the use of the same Gaussian parameters for all signal modes introduces only negligible systematic corrections. We assume that the fake D backgrounds found in the m_D sideband have the same final states as the signal and

we fit these contributions with the same Gaussian parametrization.

The fake D background is assumed to not violate CP and is therefore split equally between the B^- and B^+ subsamples. This assumption is consistent with results from our simulations and is considered further when we discuss the systematic uncertainties. The fit results are shown graphically in Fig. 2 and numerically in Table I. Table II records the number of events measured for each individual D decay mode.

Although most systematic uncertainties cancel for $\mathcal{A}_{CP}$, a charge asymmetry inherent to the detector or data processing may exist. We quote the results from the study carried out in Ref. [24], where we used $B^- \to D^0\pi^-$ (with D^0 decays into CP or non-CP eigenstates) events from control samples of data and simulation to measure the charge asymmetry. An average charge asymmetry of $A_{\rm ch} = (-1.6 \pm 0.6)\%$ was measured. We add linearly the central value and one-standard deviation in the most conservative direction to assign a systematic uncertainty of 0.022. The second substantial systematic effect is a possible CP asymmetry in the fake D background that cannot be excluded due to CP violation in charmless B decays. If there is an asymmetry $\mathcal{A}_{\text{fake }D}$, then the systematic uncertainty on $\mathcal{A}_{CP}$ is $\mathcal{A}_{\text{fake }D} \times b/c$, where b is the contribution of the fake D background and c the signal yield. Assuming conservatively that $|\mathcal{A}_{\text{fake }D}| \leq 0.5$, we obtain systematic uncertainties of ± 0.003 and ± 0.040 on $\mathcal{A}_{CP+}$ and $\mathcal{A}_{CP-}$, respectively. Note that since we do not observe any fake D background in $CP-$ modes, we use the statistical uncertainty of the signal yield from the fit to estimate this systematic uncertainty.

Since $\mathcal{R}_{CP}$ is a ratio of rates of processes with different final states of the D, we must consider the uncertainties affecting the selection algorithms for the different D channels. This results in small corrections which account for the difference between the actual detector response and the simulation model. The main effects stem from the approximate modeling of the tracking efficiency (a correction of 0.4% per pion track coming from a K^0_S and 0.2% per kaon and pion track coming from other candidates), the K^0_S

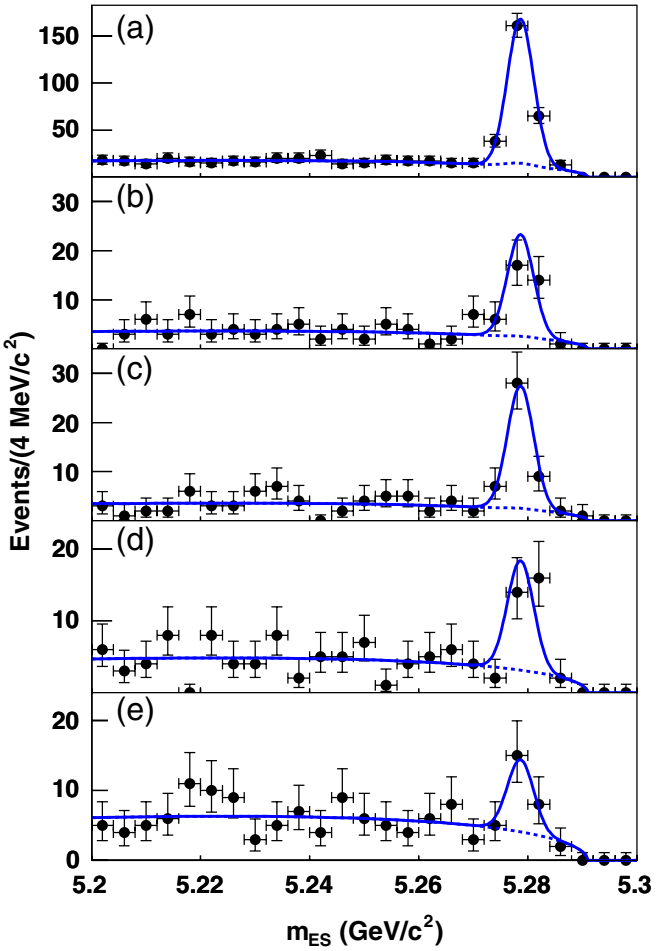

FIG. 2 (color online). Distributions of $m_{\rm ES}$ in the signal region for (a) the non-CP modes in $B^\pm$ decays, (b) the $CP+$ modes in B^+, and (c) B^- decays and (d) the $CP-$ modes in B^+ and (e) B^- decays. The dashed curve indicates the total background contributions, which include the fake D backgrounds.

TABLE I. Results from the fit. For each GLW D mode, we give the number of measured signal events, the fake D contribution, $\mathcal{A}_{CP}$, and $\mathcal{R}_{CP}$. The fake D contribution is calculated by scaling the number of fake D events found in the m_D sideband region to the signal region. The uncertainties are statistical only. We also show the number of measured signal events split by the B charge for $CP+$ and $CP-$ modes.

	# Signal	# Fake D	$\mathcal{A}_{CP}$	$\mathcal{R}_{CP}$
Non-CP	231 ± 17	5.0		
$CP+$	68.6 ± 9.2	0.3	0.09 ± 0.13	2.17 ± 0.35
(B^+)	31.2 ± 6.2			
(B^-)	37.4 ± 6.8			
$CP-$	38.5 ± 7.0	0.0	-0.23 ± 0.21	1.03 ± 0.27
(B^+)	23.0 ± 4.8			
(B^-)	15.5 ± 5.2			

TABLE II. Number of signal events from the GLW fit for individual D decay modes studied in this analysis. We also provide the selection efficiencies (in %) and total correction factors (ϵ_c). The uncertainties are statistical only.

	# Signal	Selection Efficiency (%)	$\epsilon_c(10^{-4})$
Non-CP			
$K^-\pi^+$	231 ± 17	12.76 ± 0.09	48.48 ± 0.96
$CP+$			
K^+K^-	41 ± 7	12.78 ± 0.05	4.90 ± 0.16
$\pi^+\pi^-$	28 ± 6	12.34 ± 0.05	1.72 ± 0.11
$CP-$			
$K^0_S\pi^0$	21 ± 7	5.59 ± 0.03	4.10 ± 0.50
$K^0_S\phi$	8 ± 3	8.90 ± 0.04	1.30 ± 0.11
$K^0_S\omega$	9 ± 4	2.35 ± 0.02	1.49 ± 0.30

reconstruction efficiency for $CP-$ modes of the D^0 (1.3% per K^0_S in $K^0_S\phi$ mode and 2.0% in $K^0_S\pi^0$ and $K^0_S\omega$), the π^0 reconstruction efficiency for the $K^0_S\pi^0$ and $K^0_S[\pi^+\pi^-\pi^0]_\omega$ channels (3%), and the efficiency and misidentification probabilities from the particle identification (2% per track). The corrections are calculated by comparing data and Monte Carlo using high statistics and high-purity samples. Charged kaon and pion samples obtained from D-meson decays ($D^{*+} \to D^0\pi^+$) are used for particle-identification corrections. For tracking corrections, we use τ-pair events where one τ decays to a muon and two neutrinos and the other decays to $\rho^0 h\nu$ where h is a K or a π. $B^0 \to \phi K^0_S$ and $B^0 \to \pi^+ D^-(D^- \to K^0_S\pi^-)$ decays are used for K^0_S corrections, and π^0 correction factors are calculated using $\tau \to \rho\nu$ and $\tau \to \pi\nu$ samples. The total correction factors, which also include branching fractions and selection efficiencies, used in the calculation of $\mathcal{R}_{CP\pm}$ [Eq. (3)] are given in Table II. R_{CP+} (R_{CP-}) is calculated using the number of detected signal events corrected by the linear sum of the $CP+$ ($CP-$) correction factors. Altogether, the systematic uncertainties due to the corrections equal ± 0.078 and ± 0.100 for $\mathcal{R}_{CP+}$ and $\mathcal{R}_{CP-}$, respectively. The uncertainties on the measured branching fractions [3] and efficiencies for different D decay modes, are included in the calculation of the systematic errors due to these corrections.

Another systematic correction applied to the $CP-$ measurements arises from a possible $CP+$ background in the $K^0_S\phi$ and $K^0_S\omega$ channels. In this case, the observed quantities $\mathcal{A}^{\rm obs}_{CP-}$ and $\mathcal{R}^{\rm obs}_{CP-}$ are corrected:

$$\mathcal{A}_{CP-} = (1+\epsilon)\mathcal{A}^{\rm obs}_{CP-} - \epsilon\mathcal{A}_{CP+};$$
$$\mathcal{R}_{CP-} = \frac{\mathcal{R}^{\rm obs}_{CP-}}{(1+\epsilon)},$$

where ϵ is the ratio of $CP+$ background to $CP-$ signal. An investigation of the $D^0 \to K^-K^+K^0_S$ Dalitz plot [25] indicates that the dominant background for $D^0 \to K^0_S\phi$ comes from the decay $a_0(980) \to K^+K^-$, at the level of $(25 \pm 1)\%$ of the size of the ϕK^0_S signal. We have no information for the ωK^0_S channel and assume $(30 \pm 30)\%$ of $CP+$ background contamination. The $K^0_S\pi^0$ mode has no $CP+$ background. The value of ϵ for the combination of $CP-$ modes is $(11 \pm 7)\%$. The systematic uncertainty associated with this effect is ± 0.02 and ± 0.06 for $\mathcal{A}_{CP-}$ and $\mathcal{R}_{CP-}$, respectively.

To account for the nonresonant $K^0_S\pi^-$ pairs in the K^* mass range we study a model that incorporates S-wave and P-wave pairs in both the $b \to c\bar{u}s$ and $b \to u\bar{c}s$ amplitudes. The P-wave mass dependence is described by a single relativistic Breit-Wigner while the S-wave component is assumed to be a complex constant. It is expected that higher order partial waves will not contribute significantly and therefore they are neglected in the model. We also assume that the same relative amount of S and P wave is present in the $b \to c\bar{u}s$ and $b \to u\bar{c}s$ amplitudes. The amount of S wave present in the favored $b \to c\bar{u}s$ amplitude is determined directly from the data by fitting the angular distribution of the $K^0_S\pi$ system in the K^* mass region, accounting for interference [26]. From this fit we determine that the number of non-K^* $K_S\pi^-$ events is $(4 \pm 1)\%$ of the measured signal events. To estimate the systematic uncertainties due to this source we vary all the strong phases between 0 and 2π and calculate the maximum deviation between the S-wave model and the expectation if there were no nonresonant contribution for both $\mathcal{A}_{CP\pm}$ [Eq. (2)] and $\mathcal{R}_{CP\pm}$ [Eq. (1)]. This background induces systematic variations of ± 0.051 for $\mathcal{A}_{CP\pm}$ and ± 0.035 for $\mathcal{R}_{CP\pm}$.

TABLE III. Summary of systematic uncertainties for the GLW analysis.

Source	$\delta\mathcal{A}_{CP+}$	$\delta\mathcal{A}_{CP-}$	$\delta\mathcal{R}_{CP+}$	$\delta\mathcal{R}_{CP-}$
Detection asymmetry	0.022	0.022	...	...
Nonresonant $K^0_s\pi^-$ bkg.	0.051	0.051	0.035	0.035
Same-final-state bkg.	...	0.019	...	0.061
Asymmetry in fake D^0 bkg.	0.003	0.040	...	...
Efficiency correction	...	...	0.078	0.100
Same $\mathcal{G}$ and $\mathcal{A}$ shape	0.003	0.013	0.009	0.025
Total systematic uncertainty	0.056	0.072	0.086	0.125

The last systematic uncertainty is due to the assumption that the parameters of the Gaussian and ARGUS functions are the same throughout the signal region, ΔE and m_D sidebands. We estimate the uncertainties by varying the width and mean of the Gaussian and ξ of the ARGUS by their corresponding statistical uncertainties obtained from the fit. All the systematic uncertainties are listed in Table III. We add them in quadrature and quote the final results:

$$\mathcal{A}_{CP+} = 0.09 \pm 0.13(\text{stat.}) \pm 0.06(\text{syst.})$$
$$\mathcal{A}_{CP-} = -0.23 \pm 0.21(\text{stat.}) \pm 0.07(\text{syst.})$$
$$\mathcal{R}_{CP+} = 2.17 \pm 0.35(\text{stat.}) \pm 0.09(\text{syst.})$$
$$\mathcal{R}_{CP-} = 1.03 \pm 0.27(\text{stat.}) \pm 0.13(\text{syst.}).$$

These results can also be expressed in terms of $x_\pm$ defined in Eq. (4):

$$x_+ = 0.21 \pm 0.14(\text{stat.}) \pm 0.05(\text{syst.}),$$
$$x_- = 0.40 \pm 0.14(\text{stat.}) \pm 0.05(\text{syst.}),$$

where the $CP+$ pollution systematic effects are included. Including these effects increased x_+ and x_- by 0.035 ± 0.024 and 0.023 ± 0.017, respectively.

IV. THE ADS ANALYSIS

In the ADS analysis we only use D decays with a charged kaon and pion in the final state and K^{*-} decays

to $K^0_S\pi^-$ followed by $K^0_S \to \pi^+\pi^-$. The ADS event selection criteria and procedures are nearly identical to those used for the GLW analysis. However due to the small value of r_D the yield of interesting ADS events (i.e., $B^- \to [K^+\pi^-]_D K^{*-}$ and $B^+ \to [K^-\pi^+]_D K^{*+}$) is expected to be smaller than for the GLW analysis. Therefore in order to reduce the background in the ADS analysis the K^0_S invariant mass window is narrowed to 10 MeV/c^2 and the K^{*-} invariant mass cut is reduced to 55 MeV/c^2. A neural network using the same variables as in the GLW analysis is trained on ADS signal and continuum Monte Carlo events and verified using off-peak continuum data. The separation between signal and continuum background is shown in Fig. 3. We select candidates, both right and wrong sign, with neural network output above 0.85. All other K^0_S, K^{*-}, and continuum suppression criteria are the same as those used in the GLW analysis.

$D \to K^-\pi^+$ and $K^+\pi^-$ candidates are used in this analysis. Candidates that have an invariant mass within 18 MeV/c^2 (2.5 standard deviations) of the nominal D^0 mass [3] are kept for further study. We require kaon candidates to pass the same particle-identification criteria as imposed in the GLW analysis.

We identify B-meson candidates using the beam-energy-substituted mass $m_{\rm ES}$ and the energy difference ΔE. For this analysis signal candidates must satisfy $|\Delta E| \leq 25$ MeV. The efficiency to detect a $B^- \to D^0 K^{*-}$ signal event where $D^0 \to K\pi$, after all criteria are imposed, is $(9.6 \pm 0.1)\%$ and is the same for $D^0 \to K^-\pi^+$ and $D^0 \to K^+\pi^-$. In 1.8% of the events we find more than one suitable candidate. In such cases we choose the candidate with the smallest χ^2 defined in Eq. (7). Simulations show that negligible bias is introduced by this choice and the correct candidate is picked about 88% of the time.

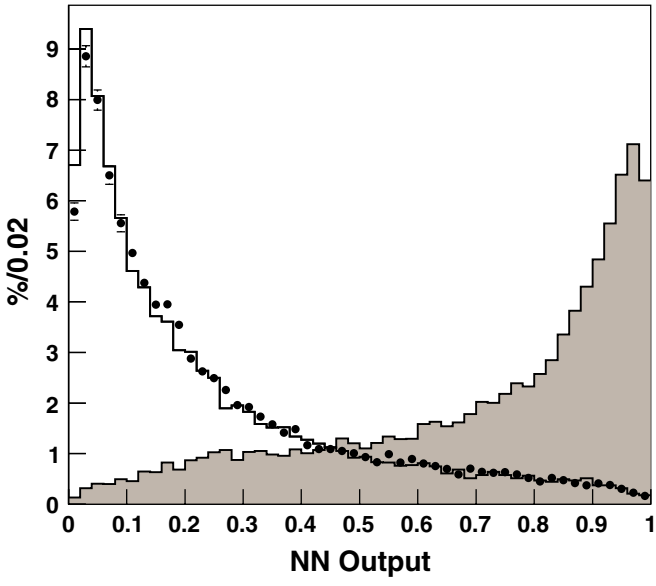

FIG. 3 (color online). Neural network (NN) output and result of the NN verification for the ADS analysis (see text). The samples used to produce the output are shown as histograms. The signal (Monte Carlo simulation) is the shaded histogram peaking near 1; the continuum (Monte Carlo simulation) is the histogram peaking near 0. The off-peak data used to check the NN are overlaid as data points.

We study various potential sources of background using a combination of Monte Carlo simulation and data events. Two sources of background are identified in large samples of simulated $B\bar{B}$ events. One source is $B^- \to D^0 K^0_S \pi^-$ production where the $K^0_S\pi^-$ is nonresonant and has an invariant mass in the K^{*-} mass window. This background is discussed later. The second background (peaking background) includes instances where a favored decay (e.g., $B^- \to [K^-\pi^+]_D K^{*-}$) contributes to fake candidates for the suppressed decay (i.e., $B^+ \to [K^-\pi^+]_D K^{*+}$). The most common way for this to occur is for a π^+ from the rest of the event to be substituted for the π^- in the K^{*-} candidate. Other sources of peaking background include double particle-identification failure in signal events that results in $D^0 \to K^-\pi^+$ being reconstructed as $D^0 \to \pi^- K^+$, or the kaon from the D^0 being interchanged with the charged pion from the K^*. We quantify this background with the ratio of the signal efficiency of wrong-sign decay to right-sign decay multiplied by the right-sign yield from data. The total size of this right-sign pollution is estimated to be 2.4 ± 0.3 events. Another class of backgrounds is charmless decays with the same final state as the signal (e.g., $B^- \to K^{*-}K^+\pi^-$). Since the branching fractions for many of these charmless decays have not been measured or are poorly measured, we use the D sideband to estimate the contamination from this source. From a fit to the $m_{\rm ES}$ distribution using candidates in the D sideband we find 0.0 ± 1.1 events. We take the 1.1 events as the contribution to the systematic uncertainty from this source.

Signal yields are determined from an unbinned extended maximum likelihood fit to the $m_{\rm ES}$ distribution in the range $5.2 \leq m_{\rm ES} \leq 5.3$ GeV/c^2. A Gaussian function ($\mathcal{G}$) is used to describe all signal shapes while the combinatorial background is modeled with an ARGUS threshold function ($\mathcal{A}$) defined in Eq. (8). The mean and width of the Gaussian as well as the ξ parameter of the ARGUS function are determined by the fit. For the likelihood function we use $a \cdot \mathcal{A} + b \cdot \mathcal{G}$ where a is the number of background events and b the number of signal events. We correct b for the right-sign peaking background previously discussed (2.4 ± 0.3 events).

In Fig. 4 we show the results of a simultaneous fit to $B^- \to [K^+\pi^-]_D K^{*-}$ and $B^- \to [K^-\pi^+]_D K^{*-}$ candidates that satisfy all selection criteria. It is in the wrong-sign decays that the interference we study takes place. Therefore in Fig. 5 we display the same fit separately for the wrong-sign decays of the B^+ and the B^- mesons. The results of the maximum likelihood fit are $\mathcal{R}_{\rm ADS} = 0.066 \pm 0.031$, $\mathcal{A}_{\rm ADS} = -0.34 \pm 0.43$, and $172.9 \pm 14.5 B^- \to [K^-\pi^+]_D K^{*-}$ right-sign events. Expressed in terms of

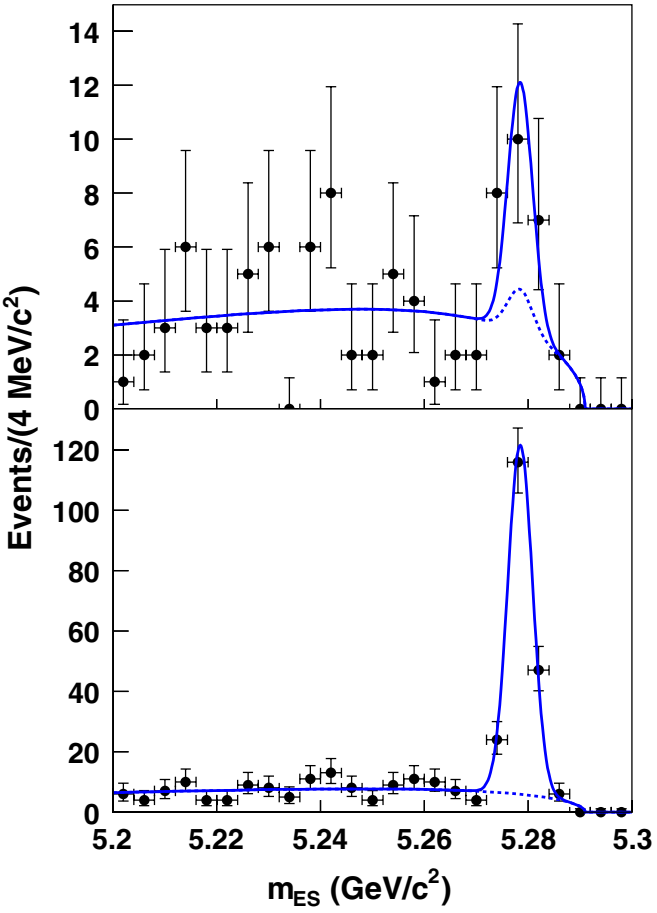

FIG. 4 (color online). Distributions of $m_{\rm ES}$ for the wrong-sign (top) and right-sign (bottom) decays. These decay categories are defined in the text. The dashed curve indicates the total background contribution. It also includes the right-sign peaking background estimated from a Monte Carlo study for the wrong-sign (top) decays. The curves result from a simultaneous fit to these distributions with identical PDFs for both samples.

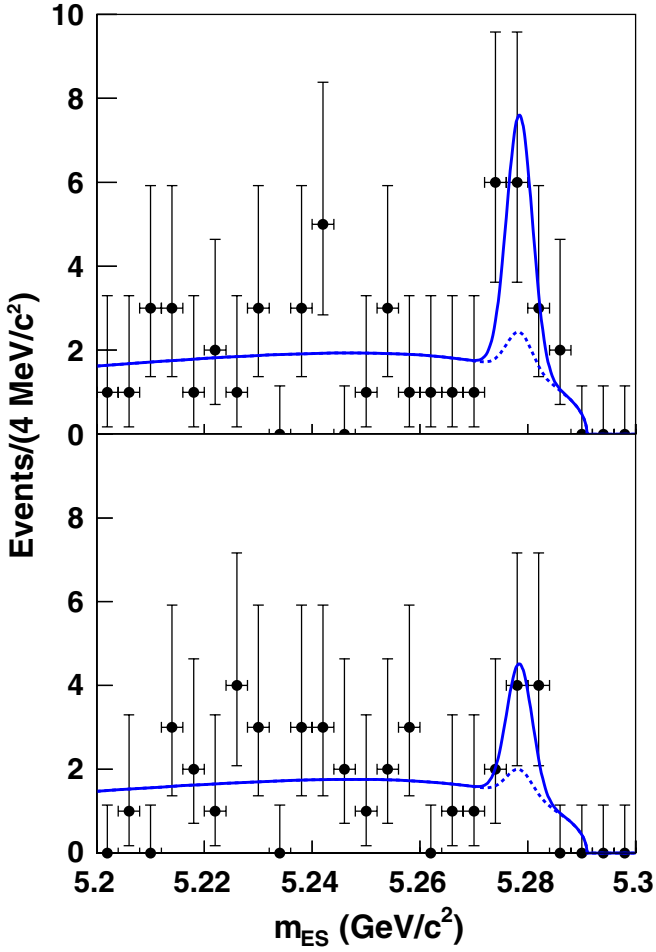

FIG. 5 (color online). The wrong-sign sample shown in the top plot of Fig. 4 split by charge. Upper plot shows the $m_{\rm ES}$ distribution of the $B^+ \to [K^-\pi^+]_D K^{*+}$ decays while lower plot presents the same for the $B^- \to [K^+\pi^-]_D K^{*-}$ decays. The dashed curve indicates the total background contribution which includes the right-sign peaking background.

the wrong-sign yield, the fit result is 11.5 ± 5.3 wrong-sign events ($3.8 \pm 3.4 B^- \to [K^+\pi^-]_D K^{*-}$ and 7.7 ± 4.2 $B^+ \to [K^-\pi^+]_D K^{*+}$ events). The uncertainties are statistical only. The correlation between $\mathcal{R}_{\rm ADS}$ and $\mathcal{A}_{\rm ADS}$ is insignificant.

We summarize in Table IV the systematic uncertainties relevant to this analysis. Since both $\mathcal{R}_{\rm ADS}$ and $\mathcal{A}_{\rm ADS}$ are ratios of similar quantities, most potential sources of systematic uncertainties cancel.

For the estimation of the detection-efficiency asymmetry we use the previously mentioned results from the study carried out in Ref. [24]. We add linearly the central value and one-standard deviation in the most conservative direction to assign a systematic uncertainty of $\delta A_{\rm ch} = \pm 0.022$ to the $\mathcal{A}_{\rm ADS}$ measurement. To a good approximation the systematic uncertainty in $\mathcal{R}_{\rm ADS}$ due to this source is $\delta\mathcal{R}_{\rm ADS} = \mathcal{R}_{\rm ADS} \cdot \mathcal{A}_{\rm ADS} \cdot \delta A_{\rm ch}$.

To estimate the systematic uncertainty on $\mathcal{A}_{\rm ADS}$ and $\mathcal{R}_{\rm ADS}$ due to the peaking background, we use the statistical uncertainty on this quantity, ± 0.3 events. With approximately $12 B^- \to [K^+\pi^-]_D K^{*-}$ events and $173 B^- \to [K^-\pi^+]_D K^{*-}$ events this source contributes ± 0.002 and ± 0.024 to the systematic uncertainties on $\mathcal{R}_{\rm ADS}$ and $\mathcal{A}_{\rm ADS}$, respectively. Similarly, the 1.1 events uncertainty on the same-final-state background leads to systematic uncertainties of ± 0.0061 and ± 0.091 on $\mathcal{R}_{\rm ADS}$ and $\mathcal{A}_{\rm ADS}$, respectively.

TABLE IV. Summary of ADS systematic uncertainties.

Source	$\delta\mathcal{R}_{\rm ADS}$	$\delta\mathcal{A}_{\rm ADS}$
Detection asymmetry	± 0.0005	± 0.022
Peaking bkg.	± 0.0020	± 0.024
Same-final-state bkg.	± 0.0061	± 0.091
Nonresonant $K^0_s\pi^-$ bkg.	± 0.0073	± 0.126
Total systematic uncertainty	± 0.0097	± 0.159

As in Sec. III, we need to estimate the systematic effect due to the nonresonant $K^0_S\pi^-$ pairs in the K^* mass range. We follow the same procedure discussed in Sec. III. After adding in quadrature the individual systematic uncertainty contributions, listed in Table IV, we find:

$$\mathcal{A}_{\rm ADS} = -0.34 \pm 0.43(\text{stat.}) \pm 0.16(\text{syst.})$$
$$\mathcal{R}_{\rm ADS} = 0.066 \pm 0.031(\text{stat.}) \pm 0.010(\text{syst.})$$

V. COMBINED RESULTS

We use the GLW and ADS results and a frequentist statistical approach [27] to extract information on r_B and γ. In this technique, a χ^2 is calculated using the differences between the measured and theoretical values and the statistical and systematic errors of the six measured quantities. The values of r_D and δ_D are taken from Ref. [12], while we allow $0 \le r_B \le 1$, $0° \le \gamma \le 180°$, and $0° \le \delta_B \le 360°$. The minimum of the χ^2 for the r_B, γ, and δ_B parameter space is calculated first ($\chi^2_{\rm min}$). We then scan the range of r_B and γ minimizing the χ^2 ($\chi^2_{\rm m}$) by varying δ_B. A confidence level for each value of r_B and γ is calculated using $\Delta\chi^2 = \chi^2_{\rm m} - \chi^2_{\rm min}$ and 1 degree of freedom. We assume Gaussian measurement uncertainties and confirm this assumption using simulations. In Fig. 6 we show the 95% confidence level contours for r_B versus γ as well as the 68% confidence level contours for the GLW and the combined GLW and ADS analysis (striped areas).

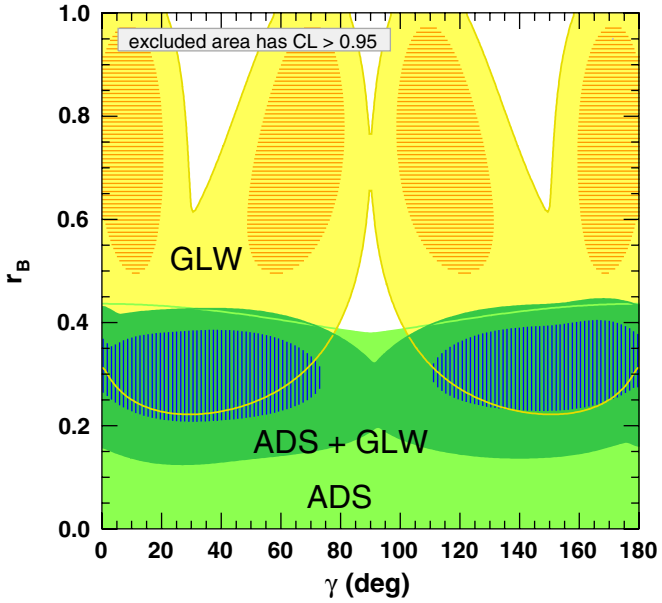

FIG. 6 (color online). 95% confidence level contours from a two dimensional scan of γ versus r_B from the $B^- \to DK^{*-}$ GLW and ADS measurements. Also shown are the 68% confidence level regions (striped areas) for the GLW and the fit which uses both the GLW and ADS measurements. r_D and δ_D are from Ref. [12].

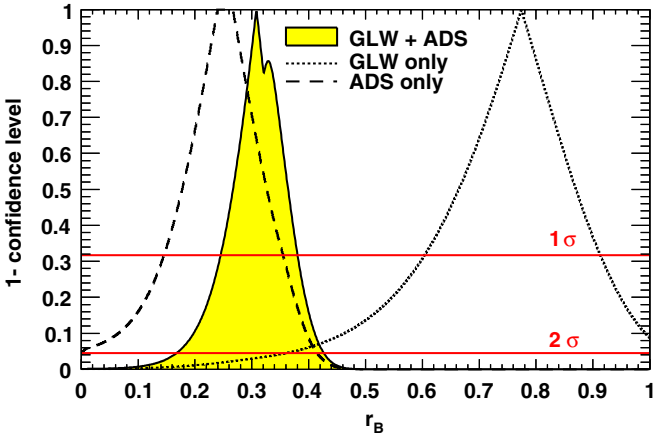

FIG. 7 (color online). Constraints on r_B from the $B^- \to DK^{*-}$ GLW and ADS measurements. The dashed (dotted) curve shows 1 minus the confidence level to exclude the abscissa value as a function of r_B derived from the GLW (ADS) measurements. The GLW + ADS result (solid line and shaded area) is from a fit which uses both the GLW and ADS measurements as well as r_D and δ_D from [12]. The horizontal lines show the exclusion limits at the 1 and 2 standard deviation levels.

In order to find confidence levels for r_B we use the above procedure, minimizing χ^2 with respect to γ and δ_B. The results of this calculation are shown in Fig. 7. The fit which uses both the ADS and GLW results has its minimum χ^2 at $r_B = 0.31$ with a one sigma interval of [0.24, 0.38] and a two sigma interval of [0.17, 0.43]. The value $r_B = 0$ is excluded at the 3.3 sigma level. We find similar results for r_B using the modifications to this frequentist approach discussed in Ref. [28] and using the Bayesian approach of Ref. [29].

Using the above procedure we also find confidence intervals for γ. The results of the scan in γ are shown in Fig. 8. The combined GLW + ADS analysis excludes

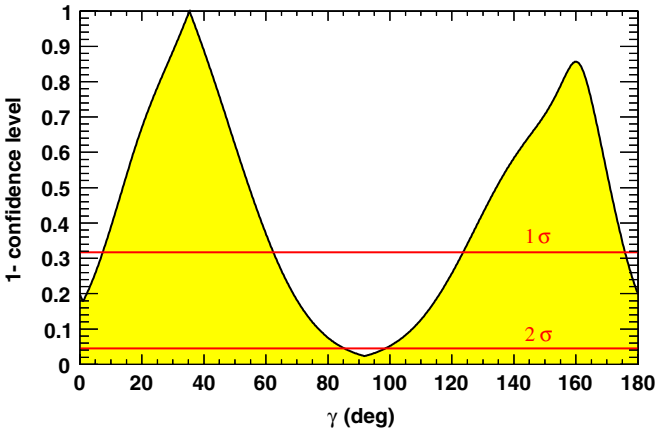

FIG. 8 (color online). Constraints on γ from a fit which uses both the $B^- \to DK^{*-}$ GLW and ADS measurements as well as r_D and δ_D from [12]. The horizontal lines show the exclusion limits at the 1 and 2 standard deviation levels.

values of γ in the regions [0, 7]°, [62, 124]°, and [175, 180]° at the one sigma level and [85, 99]° at the two sigma level. The use of the measurement of the strong phase δ_D [12] helps to resolve the ambiguities on γ and therefore explains the asymmetry in the confidence level plot shown in Fig. 8.

VI. SUMMARY

In summary, we present improved measurements of yields from $B^- \to DK^{*-}$ decays, where the neutral D-meson decays into final states of even and odd CP (GLW), and the $K^+\pi^-$ final state (ADS). We express the results as $\mathcal{R}_{CP}$, $\mathcal{A}_{CP}$, $x_\pm$, $\mathcal{R}_{\rm ADS}$, and $\mathcal{A}_{\rm ADS}$. The value $r_B = 0$ is excluded at the 3.3 sigma level. These results in combination with other GLW, ADS, and Dalitz type analyses improve our knowledge of r_B and γ.

ACKNOWLEDGMENTS

We are grateful for the extraordinary contributions of our PEP-II colleagues in achieving the excellent luminosity and machine conditions that have made this work possible. The success of this project also relies critically on the expertise and dedication of the computing organizations that support *BABAR*. The collaborating institutions wish to thank SLAC for its support and the kind hospitality extended to them. This work is supported by the US Department of Energy and National Science Foundation, the Natural Sciences and Engineering Research Council (Canada), the Commissariat à l'Energie Atomique and Institut National de Physique Nucléaire et de Physique des Particules (France), the Bundesministerium für Bildung und Forschung and Deutsche Forschungsgemeinschaft (Germany), the Istituto Nazionale di Fisica Nucleare (Italy), the Foundation for Fundamental Research on Matter (The Netherlands), the Research Council of Norway, the Ministry of Education and Science of the Russian Federation, Ministerio de Educación y Ciencia (Spain), and the Science and Technology Facilities Council (United Kingdom). Individuals have received support from the Marie-Curie IEF program (European Union) and the A. P. Sloan Foundation.

[1] N. Cabibbo, Phys. Rev. Lett. **10**, 531 (1963); M. Kobayashi and T. Maskawa, Prog. Theor. Phys. **49**, 652 (1973).
[2] *CP Violation*, edited by C. Jarlskog, Advanced Series on Directions in High Energy Physics Vol. 3 (World Scientific, Singapore, 1989).
[3] C. Amsler *et al.* (Particle Data Group), Phys. Lett. B **667**, 1 (2008).
[4] M. Gronau and D. London, Phys. Lett. B **253**, 483 (1991); M. Gronau, Phys. Rev. D **58**, 037301 (1998).
[5] M. Gronau and D. Wyler, Phys. Lett. B **265**, 172 (1991).
[6] D. Atwood, I. Dunietz, and A. Soni, Phys. Rev. Lett. **78**, 3257 (1997).
[7] A. Soffer, Phys. Rev. D **60**, 054032 (1999).
[8] Hereafter K^{*-} implies $K^*(892)^-$. In this paper we use only the $K^{*\pm} \to K^0_S\pi^\pm$, $K^0_S \to \pi^+\pi^-$ decay chain.
[9] By D we mean any linear combination of D^0 and $\bar{D}^0$.
[10] J. P. Silva and A. Soffer, Phys. Rev. D **61**, 112001 (2000); Y. Grossman, A. Soffer, and J. Zupan, Phys. Rev. D **72**, 031501(R) (2005).
[11] A. Giri, Y. Grossman, A. Soffer, and J. Zupan, Phys. Rev. D **68**, 054018 (2003); B. Aubert *et al.* (*BABAR* Collaboration), Phys. Rev. Lett. **95**, 121802 (2005).
[12] E. Barberio *et al.*, arXiv:0808.1297v3; the *BABAR* convention for δ_D differs from the one in this reference by π.
[13] M. Gronau, Phys. Lett. B **557**, 198 (2003).
[14] B. Aubert *et al.* (*BABAR* Collaboration), Phys. Rev. D **72**, 071104 (2005).
[15] B. Aubert *et al.* (*BABAR* Collaboration), Phys. Rev. D **72**, 071103 (2005).
[16] B. Aubert *et al.* (*BABAR* Collaboration), Nucl. Instrum. Methods Phys. Res., Sect. A **479**, 1 (2002).
[17] S. Agostinelli *et al.* (Geant4 Collaboration), Nucl. Instrum. Methods Phys. Res., Sect. A **506**, 250 (2003).
[18] D. Lange, Nucl. Instrum. Methods Phys. Res., Sect. A **462**, 152 (2001).
[19] T. Sjostrand, Comput. Phys. Commun. **82**, 74 (1994).
[20] B. Aubert *et al.* (*BABAR* Collaboration), Phys. Rev. D **69**, 032004 (2004).
[21] B. Aubert *et al.* (*BABAR* Collaboration), Phys. Rev. Lett. **89**, 281802 (2002).
[22] G. C. Fox and S. Wolfram, Phys. Rev. Lett. **41**, 1581 (1978).
[23] H. Albrecht *et al.* (ARGUS Collaboration), Phys. Lett. B **185**, 218 (1987); **241**, 278 (1990).
[24] B. Aubert *et al.* (*BABAR* Collaboration), Phys. Rev. D **77**, 111102 (2008).
[25] B. Aubert *et al.* (*BABAR* Collaboration), Phys. Rev. D **72**, 052008 (2005).
[26] B. Aubert *et al.* (*BABAR* Collaboration), Phys. Rev. D **73**, 111104 (2006).
[27] J. Charles *et al.*, Eur. Phys. J. C **41**, 1 (2005).
[28] B. Aubert *et al.* (*BABAR* Collaboration), Phys. Rev. D **78**, 034023 (2008).
[29] M. Ciuchini *et al.*, J. High Energy Phys. 07 (2005) 28.